Journal of Alloys and Compounds 574 (2013) 124–130

Contents lists available at SciVerse ScienceDirect

Journal of Alloys and Compounds

journal homepage: www.elsevier.com/locate/jalcom

# Structural parameters, band-gap bowings and phase diagrams of zinc-blende $Sc_{1-x}In_xP$ ternary alloys: A FP-LAPW study

William López-Pérez [a,*], Nicolás Simon-Olivera [a], Javier Molina-Coronell [b], Alvaro González-García [a], Rafael González-Hernández [a]

[a] Grupo de Investigación en Física Aplicada, Departamento de Física, Universidad del Norte, Barranquilla, Colombia
[b] Departamento de Ciencias Básicas, Universidad de la Costa, Barranquilla, Colombia

ARTICLE INFO

*Article history:*
Received 7 December 2012
Accepted 11 March 2013
Available online 6 April 2013

*Keywords:*
Density functional calculations
Structural properties
Electronic properties
Thermodynamic properties

ABSTRACT

Using first-principles total-energy calculations, we investigate the structural, electronic and thermodynamic properties of the cubic $Sc_{1-x}In_xP$ semiconducting alloys. The calculations are based on the full-potential linearized-augmented plane wave (FP-LAPW) method within density functional theory (DFT). The exchange–correlation effect is treated by both local-density approximation (LDA) and generalized-gradient approximation (GGA). In the latter approach, both Perdew-Burke-Ernzerhof (PBE) and EngelVosko (EV) functional of the exchange–correlation energy were used. The effect of atomic composition on structural parameters, band-gap energy, mixing enthalpy and phase diagram was analyzed for $x = 0$, 0.25, 0.5, 0.75, 1. Lattice constant, bulk modulus, and band-gap energy for zinc-blende $Sc_{1-x}In_xP$ alloys show nonlinear dependence on the aluminium composition $x$. Deviations of the lattice constant from Vegard's law, and deviations of the bulk modulus and band-gap energy from linear concentration dependence (LCD) were found. The variation of the calculated equilibrium lattice constant versus indium concentration shows a small deviation from Vegard's law with upward bowing parameter of −0.043 Å and −0.058 Å for PBE and LDA, respectively. The bulk modulus as a function of indium composition shows a small deviation from the linear concentration dependence (LCD) with upward bowing equal to −0.790 GPa using PBE, and with net downward bowing of 0.847 GPa using LDA. The results show that the band gap undergoes a direct ($X \rightarrow X$)-to-direct ($\Gamma \rightarrow \Gamma$) transition at a given indium composition $x$. The physical origin of the band-gap bowing in zinc-blende $Sc_{1-x}In_xP$ semiconducting alloys was investigated. The calculated excess mixing enthalpy is positive over the entire indium composition range.



## 1. Introduction

The III-phosphides have attracted considerable interest because of their useful electronic and optical properties. These materials are important for the production of electronic and optoelectronic devices, e.g., InP is a direct-gap semiconductor of great technological interest, because it serves as the substrate for most optoelectronic devices [1–3]. This binary compound is especially important for the design of solar cells, transferred-electron devices, communication devices, anode materials for lithium-ion batteries and high-performance computing [4–9]. At ambient conditions, the InP crystallizes in zinc-blende structure (space group $F\bar{4}3m$) with a lattice constant of 5.869 Å [1,10–12]. An experimental study on InP shows a low-temperature direct band-gap of 1.423 eV [13]. On the other hand, there are few experimental works on the structural and optical properties of ScP binary compound. A X-ray measurement has shown that ScP crystallizes in the NaCl (B1) structure with a lattice constant of 5.309 Å at room temperature [14]. On the theoretical side, because of their extensive applications, a great deal of theoretical effort has been devoted to the study of the energy band structures and related properties of these materials. In recent years, the physical properties of InP have been reported in a large number of theoretical studies, performed to confirm the experimental measurements [15–20]. There are several theoretical works on the structural, electronic, thermodynamic, dynamical and optical properties of ScP compound [21–23]. In these studies, using first-principles calculations the authors describe the structural and electronic properties in the ground state of ScP, observing a metallic character in the B1 phase (NaCl). They found that a transition from rocksalt (NaCl) to cesium chloride (CsCl) structure is possible at high pressure (330 GPa). The zinc-blende phase was also investigated, and it was found that this phase has a semiconducting behavior with a wide band gap. From these studies it appears that zinc-blende ScP is a good lattice match for zinc-blende III-A phosphides.

On the other hand, IIIV ternary semiconductor alloys are promising candidates for many device applications such as

* Corresponding author. Tel.: +57 53509509; fax: +57 53598852.
*E-mail address:* wlopez@uninorte.edu.co (W. López-Pérez).

0925-8388/$ - see front matter © 2013 Elsevier B.V. All rights reserved.
http://dx.doi.org/10.1016/j.jallcom.2013.03.108

high-speed electronic and long wavelength photonic devices because their band-gaps cover a wide spectral range [24,25]. The variation of atomic composition is a way of controlling the magnitude of the forbidden gap and other parameters necessary to optimize and extend the applications of semiconducting alloys [26]. Usually, one comes to the doping of semiconductor material as the most efficient way to increase the free carriers concentration by producing an energy level in a forbidden gap energy, which modifies the optical and electronic properties of the material. As it is known, the inclusion of a third atom of another class in a binary material (e.g. ScP) alters the physical and chemical properties because it causes changes in the bonds. The compositional dependence of the electronic properties of ternary alloys is relevant in the design and manufacture of electronic and opto-electronics devices. Some promising candidates for this compositional modulation are phosphorus-based ternary alloys. Thus, a precise knowledge of the structural, electronic and thermodynamic properties, and their compositional dependence in these semiconductor alloys is necessary to evaluate their expectable range of applications. This has motivated recent studies on theoretical characterizations of $In_xGa_{1-x}P$ and $Al_xIn_{1-x}P$ ternary alloys [27,28]. However, there is a ternary phosphides group that theoretically and experimentally have not been studied, we refer to compounds ScP:In. In this regard, we have performed a theoretical research of the structural, electronic and thermodynamic properties of zinc-blende $Sc_{1-x}Al_xAs$ alloys performing first-principles total energy calculations within DFT for indium concentrations of $x = 0, 0.25, 0.5, 0.75, 1$.

## 2. Computational methods

To model the disordered zinc-blende $Sc_{1-x}In_xP$ ternary alloys, we employed special quasi-random structures (SQSs) [29]. SQS optimize the arrangement of the Sc and In atoms for a given number of lattice sites, such that the structure as a whole mimics the lowest order correlation functions of an infinite random alloy. SQS model is based on the fact that many physical properties of solids are characterized by microscopic length scales and local randomness of alloys, and are not affected by the change of the large scale randomness of alloys. In this study the alloys are modeled at some selected compositions with ordered structures described in terms of periodically repeated supercells. SQS scheme allows us to select the simplest unit cell for each analyzed composition. For the compositions $x = 0.25$, 0.5 and 0.75, the simplest structure is an eight-atom simple cubic lattice. In order to obtain the structural, electronic and thermodynamic properties of $Sc_{1-x}In_xP$ alloys, we have performed total-energy and electronic-structure calculations using the first-principles FP-LAPW method as implemented in the WIEN2k code [30] within the framework of DFT [31,32]. In this method, a basis is adapted to the problem by dividing the unit cell into non-overlapping muffin-tin (MT) spheres surrounding the atomic sites and an interstitial region. Basis functions were expanded in combinations of spherical harmonic functions inside non-overlapping MT spheres and in Fourier series in the interstitial region. To solve the Kohn–Sham equations, the exchange–correlation potential for structural and electronic properties was calculated using both LDA and GGA approaches. The LDA functional from Perdew and Wang [33] was used to calculate both structural and electronic properties. In the GGA approach, the PBE parametrization [34] was used to obtain both structural and electronic information, while EV functional [35] was only used to calculate the band-gap energy. The electron density is obtained by summing over all occupied Kohn–Sham orbitals which permits to know the ground state of the system. We have adopted the values of 1.60, 1.65 and 2.40 u.a for P, Sc and In atoms, respectively, as muffin-tin radius ($R_{MT}$). A mesh of 64 special k-points for binary compounds and 27 special k-points for ternary alloys were considered in the irreducible wedge of the Brilloiun zone. The electronic configurations for Sc, In and P are Sc:[Ar]$3d^14s^2$, In:[Kr]$4d^{10}5s^25p^1$ and P:[Ne]$3s^23p^3$. In the calculations, the sub-shells of the noble-gas cores were distinguished from the sub-shells of valence electrons given explicitly. The separation energy among the valence and core states is $-6.0Ry$. The maximum l value for the wave functions expansion inside spheres was confined to $l_{max} = 10$, while the charge density was expanded up to $G_{max} = 14(Ry)^{1/2}$. The wave functions in the interstitial region are expanded in plane waves up to the cutoff value $K_{max} = 8.0/R_{mt}$, where $R_{mt}$ is the smallest atomic sphere radii inside the cell and $K_{max}$ is the cutoff for the basis function wave vector. The convergence criterion in energy was of $0.1mRy$. Structural parameters were computed by fitting the total energy versus volume to the Murnaghan's equation of state [36]. Subsequently, using LDA, PBE and EV functionals, the band structure at equilibrium volume of zinc-blende $Sc_{1-x}In_xP$ alloys was obtained for each indium concentration $x$.

## 3. Results and discussion

### 3.1. Structural parameters versus composition

The volume of ScP and InP in both rocksalt and zinc-blende structures was optimized by calculating the total energy at least ten different volumes around an equilibrium volume, and the results were fitted to the Murnaghan's equation of state [36]. Our calculated values for the equilibrium lattice constant, equilibrium volume, bulk modulus and equilibrium energy for the binary compounds are summarized in Table 1, together with available experimental data. Pure ScP has a rocksalt structure with experimental lattice parameter $a = 5.309$ Å [14]. Our PBE results slightly overestimate this value by 0.008 Å, while LDA underestimate them by 0.108 Å. The calculated lattice constant with LDA for InP in zinc-blende phase is slightly smaller than experimental value by 0.031 Å, while PBE gives 0.099 Å above the experimental data. Thus LDA gives a bulk modulus value consistent with the experimental value. Our LDA (PBE) results show that the lattice constant for InP is 0.024 Å (0.034 Å) larger than the one for ScP in zinc-blende phase, and 0.220 Å (0.225 Å) larger in the rocksalt phase. Hence we think that it is more probable a growth of $Sc_{1-x}In_xP$ alloys in zincblende-like structure. Therefore, we carried out a comparative LDA and GGA study for zinc-blende $Sc_{1-x}In_xP$ ternary alloys.

An increase of lattice constant with the increment of indium composition is presented in Fig. 1a. Our calculated lattice constants at different indium composition of $Sc_{1-x}In_xP$ alloys, were found to vary nonlinearly with indium concentration $x$. The variation of the calculated equilibrium lattice constant versus indium concentration shows a small deviation from the Vegard's law [37] with upward bowing parameter of $-0.043$ Å and $-0.058$ Å with PBE and LDA, respectively. A small value of the deviation was expected, since the lattice constants of constituent binaries in zinc-blende phase are similar. The Vegard's law violation in semiconducting alloys has been reported experimentally [38]. Several factors contribute to the failure of Vegard's law: relative atomic radii of the elements, relative volume per valence electron in crystals of pure elements, Brillouin zone effects and electrochemical differences between elements [39]. In our study, lattice constants are increased due to the fact that ScP host lattice receives In atoms slightly greater than Sc atoms. As a consequence, the curve of $a(x)$ goes above of Vegard's law (see Fig. 1a). In Fig. 1b, we show the behavior of the bulk modulus as a function of indium composition for zinc-blende $Sc_{1-x}In_xP$ alloys, and compared to the results predicted by linear composition dependence (LCD). The PBE-calculated bulk modulus presents a significant decrease with increasing the indium composition, while the LDA-calculated bulk modulus increases slightly with increasing the indium concentration (see Fig. 1b). A slight deviation of the bulk modulus from the LCD is observed with upward bowing equal to $-0.790$ GPa using PBE, and with downward bowing of 0.847 GPa using LDA. This might be mainly due to the small mismatch between the bulk modulus of InP and ScP in zinc-blende phase. In Fig. 1, the star shows that there exists a good agreement between the results of our LDA calculation and the experimental data for InP.

### 3.2. Band-gap bowing parameters

The electronic structure of zinc-blende $Sc_{1-x}In_xP$ was calculated with optimized structural parameters. In order to compare the band-gap width of zinc-blende $Sc_{1-x}In_xP$ alloys, we use LDA, PBE and EV functionals for the calculations. All these approximations underestimate the band-gap energy, but EV functional can give better values than both LDA and PBE functionals. This is due to the fact that both LDA and PBE functionals are developed for

**Table 1**
Calculated structural parameters for the binary compounds in rocksalt and zinc-blende structures at equilibrium volume. Available experimental data are also shown in parentheses for comparison. Energies and volumes are per unit formule.

| | InP (LDA) | | ScP (LDA) | | InP (PBE) | | ScP (PBE) | |
|---|---|---|---|---|---|---|---|---|
| | ZB | NaCl | ZB | NaCl | ZB | NaCl | ZB | NaCl |
| $a$ (Å) | 5.838 (5.0869)[a] | 5.421 | 5.814 | 5.201 (5.309)[b] | 5.968 (5.869)[a] | 5.542 | 5.934 | 5.317 (5.309)[b] |
| $V$ (Å$^c$) | 49.745 | 39.831 | 49.142 | 35.167 | 53.153 | 42.574 | 52.228 | 37.579 |
| $B_o$ (GPa) | 71.0 (76)[c] (71.1)[d] | 88.8 | 69.7 | 109.8 | 59.3 (76)[c] (71.1)[d] | 73.2 | 63.4 | 97.3 |
| $E_o$ (eV) | 7.66 | 7.32 | 11.11 | 12.47 | 6.09 | 5.61 | 9.77 | 10.84 |

[a] Ref. [1].
[b] Ref. [14].
[c] Ref. [10].
[d] Ref [11].

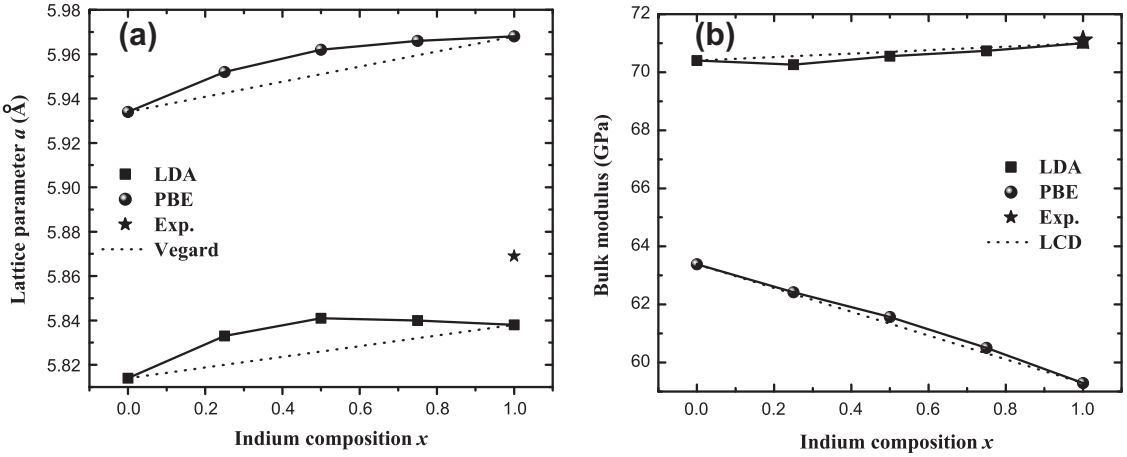


**Fig. 1.** (a) Composition dependence of the calculated lattice constant for zinc-blende $Sc_{1-x}In_xP$ ternary alloys. The calculations (solid spheres (PBE) and solid square (LDA)) are compared with the Vegard's linear tendency (dotted line). (b) Composition dependence of the bulk modulus of zinc-blende $Sc_{1-x}In_xP$ alloys. The calculations (solid spheres (PBE) and solid square (LDA)) are compared with the linear composition dependence (dotted line). The star indicates the experimental value.

**Table 2**
Calculated band-gap energies of $Sc_{1-x}In_xP$ alloys at different indium concentrations ($x$) for LDA, PBE and EV functionals. All energy values are in eV.

| $x$ | $X \to X$ | | | $\Gamma \to \Gamma$ | | | Exp. |
|---|---|---|---|---|---|---|---|
| | LDA | PBE | EV | LDA | PBE | EV | |
| 0.00 | 1.305 | 1.466 | 2.076 | 3.381 | 3.328 | 3.499 | – |
| 0.25 | 2.001 | 2.129 | 2.472 | 0.984 | 1.156 | 1.594 | – |
| 0.50 | 2.215 | 2.301 | 2.589 | 1.145 | 1.273 | 1.691 | – |
| 0.75 | 2.161 | 2.194 | 2.450 | 1.367 | 1.434 | 1.830 | – |
| 1.00 | 3.852 | 3.873 | 4.580 | 0.428 | 0.310 | 0.888 | 1.423[a] |

[a] Ref. [13].

accurate description of exchange–correlation energy, while EV functional is formulated for better treatment of exchange–correlation potential at the cost of less agreement in exchange energy [40]. Consequently, we expect the experimental band-gap energy to be larger. Our calculated band structure presents a similar behavior for any indium composition using LDA, PBE or EV functional, and the main difference is in the numerical values of the band-gap energy which were wider for the EV functional. Therefore, we presented only the calculated band-gap energies with the three functionals. Our results for zinc-blende structure yield a direct band-gap in $\Gamma \to \Gamma$ for InP, while for ScP a direct band-gap in $X \to X$ was determined. Therefore one can expect that band-gap of $Sc_{1-x}In_xP$ alloys should undergo a $X \to X$-to-$\Gamma \to \Gamma$ crossover at a certain composition $x$. To confirm this, first we have calculated the $X \to X$ and $\Gamma \to \Gamma$ band-gaps of $Sc_{1-x}In_xP$ alloys as a function of the composition $x$. These results are organized in Table 2. The EV-gap value for InP was calculated using the equilibrium lattice constant obtained with PBE. It is evident that the band-gap calculated with EV functional for InP is in good agreement with experimental data. Considering the experimental lattice constant for InP, a band-gap value (1.3 eV) still closer to the experimental data was obtained using the EV functional. It is noticeable that the $X \to X$ and $\Gamma \to \Gamma$ band-gaps of $Sc_{1-x}In_xP$ alloys show a nonlinear behavior.

Next, we describe the composition dependence of the band-gap by fitting the nonlinear variation of the $X \to X$ and $\Gamma \to \Gamma$ band-gaps by quadratic polynomial with the second-order term proportional to the bowing parameter $b$ so that

$$E_g(x) = xE_g^{\mathrm{InP}} + (1-x)E_g^{\mathrm{ScP}} - bx(1-x). \quad (1)$$

The results are also shown in Fig. 2 for three exchange–correlation functional. With the three LDA, PBE and EV functionals a downward bowing was found.

We can note that the energy $E_{\Gamma\to\Gamma}$ decreases with the increase of indium composition, while the energy $E_{X\to X}$ increases. So that $X \to X$ and $\Gamma \to \Gamma$ band-gap crossovers are located in 0.321, 0.327, 0.340 indium concentrations for LDA, PBE and EV functionals, respectively. For the three functionals, we observe a region of $X \to X$ band-gap between zero and the crossover, and another zone of $\Gamma \to \Gamma$ band-gap between the crossover and $x = 1$. We have

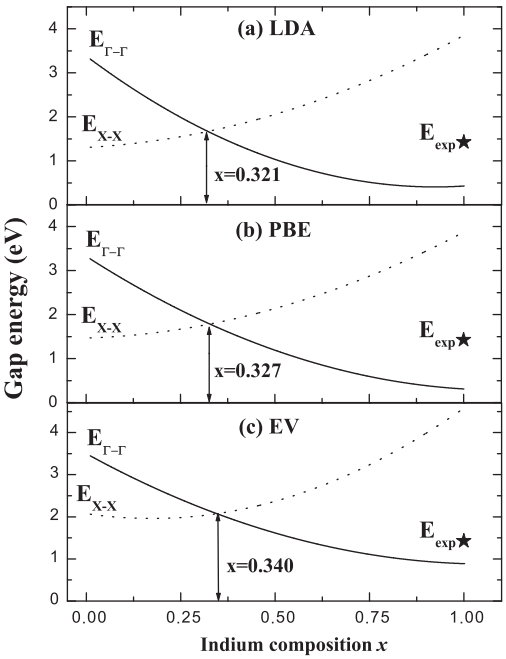


**Fig. 2.** Calculated $X \rightarrow X$ and $\Gamma \rightarrow \Gamma$ band-gap energies as a function of In-composition using the three (a) LDA, (b) PBE and (c) EV functionals. The star indicates the experimental value for InP.

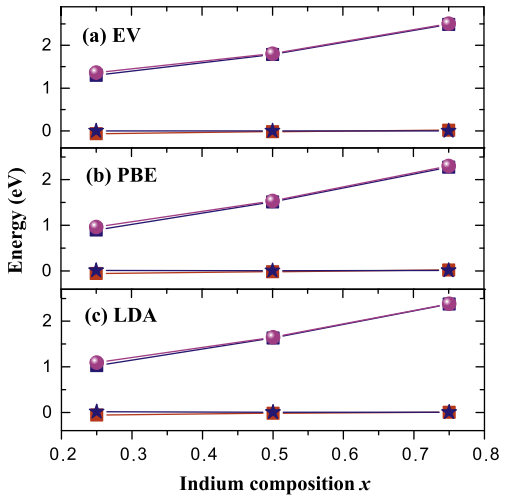


**Fig. 3.** Calculated $\Gamma \rightarrow \Gamma$ band-gap bowings and their contributions as a indium composition function using (a) EV, (b) PBE and (c) LDA functionals for zinc-blende $Sc_{1-x}In_xP$. The total band-gap bowings are indicated with pink spheres, while the contributions charge transfer $b_{CE}$ with blue solid squares, volume deformation $b_{VD}$ with red solid squares, and structural relaxation $b_{SR}$ with blue solid stars. (For interpretation of the references to color in this figure legend, the reader is referred to the web version of this article.)

identified that the band-gap value calculated with EV functional is closer to the experimental data.

In order to better understand the physical origin of the gap bowing in $Sc_{1-x}In_xP$ alloys, the bowing parameter ($b$) was calculated by using the method of Bernard and Zunger [41]. In this scheme, the $b$ parameter is decomposed into three contributions resulting from volume deformation ($b_{vd}$), charge exchange ($b_{ce}$), and structural relaxation ($b_{sr}$). At a given average composition $x$, the $Sc_{1-x}In_xP$ ternary alloy obeys the formal reaction

$$x\mathrm{InP}(a_{\mathrm{InP}}) + (1-x)\mathrm{ScP}(a_{\mathrm{ScP}}) \rightarrow \mathrm{Sc}_{1-x}\mathrm{In}_x\mathrm{P}(a_{eq}), \quad (2)$$

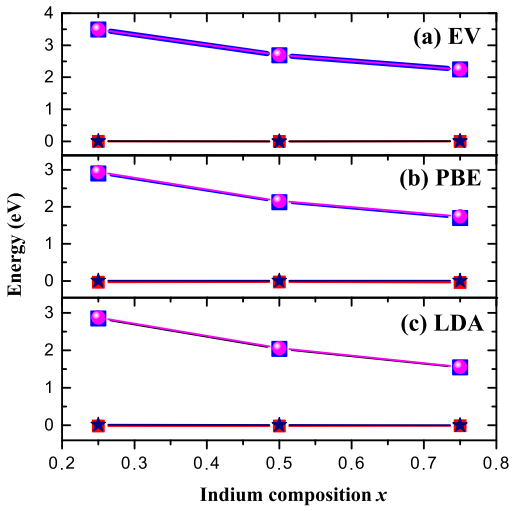


**Fig. 4.** Calculated $X \rightarrow X$ band-gap bowings and their contributions as a indium composition function using (a) EV, (b) PBE and (c) LDA functionals for zinc-blende $Sc_{1-x}In_xP$. The total band-gap bowings are indicated with pink spheres, while the contributions charge transfer $b_{CE}$ with blue solid squares, volume deformation $b_{VD}$ with red solid squares, and structural relaxation $b_{SR}$ with blue solid stars. (For interpretation of the references to color in this figure legend, the reader is referred to the web version of this article.)

where $a_{\mathrm{InP}}$ and $a_{\mathrm{ScP}}$ are the equilibrium lattice constants of the binary compounds InP and ScP, respectively, and $a_{eq}$ is the equilibrium lattice constant of the alloy at the average composition $x$. The different contributions to the band-gap bowing $b$ are attributed to volume deformation ($b_{VD}$), charge exchange ($b_{CE}$), and structural relaxation ($b_{SR}$).

The volume deformation effect on the band-gap bowing is measured by the reaction

$$\mathrm{InP}(a_{\mathrm{InP}}) + \mathrm{ScP}(a_{\mathrm{ScP}}) \rightarrow \mathrm{InP}(a) + \mathrm{ScP}(a). \quad (3)$$

Volume deformation ($b_{VD}$) represents changes in the band-gaps of the binary compounds InP and ScP by compression and expansion of their volumes, respectively. This deformation here arises from the change of their equilibrium lattice constants to the alloy value $a = a(x) = xa_{\mathrm{InP}} + (1-x)a_{\mathrm{ScP}}$, according to the reaction (3). Therefore, this contribution to the band-gap bowing is given by the expression

$$b_{VD} = \frac{E_g^{\mathrm{InP}}(a_{\mathrm{InP}}) - E_g^{\mathrm{InP}}(a)}{1-x} + \frac{E_g^{\mathrm{ScP}}(a_{\mathrm{ScP}}) - E_g^{\mathrm{ScP}}(a)}{x}. \quad (4)$$

The charge exchange effect on the band-gap bowing is determined by the reaction

$$x\mathrm{InP}(a) + (1-x)\mathrm{ScP}(a) \rightarrow \mathrm{Sc}_{1-x}\mathrm{In}_x\mathrm{P}(a), \quad (5)$$

Charge exchange ($b_{CE}$) contribution indicates the change in the band-gap when the binary components (with lattice constant $a = a(x)$) are mixed, without allowing any sublattice relaxation. In this contribution, the different bonding behaviors of the two binary constituents originate charge transfer. This contribution to the band-gap bowing can be calculated by the expression

$$b_{CE} = \frac{E_g^{\mathrm{InP}}(a)}{1-x} + \frac{E_g^{\mathrm{ScP}}(a)}{x} - \frac{E_g^{\mathrm{Sc}_{1-x}\mathrm{In}_x\mathrm{P}}(a)}{x(1-x)}. \quad (6)$$

Finally, structural relaxation ($b_{SR}$) corresponds to the reaction

$$\mathrm{Sc}_{1-x}\mathrm{In}_x\mathrm{P}(a) \rightarrow \mathrm{Sc}_{1-x}\mathrm{In}_x\mathrm{P}(a_{eq}), \quad (7)$$

where $a_{eq}$ is the optimal value of the alloy equilibrium lattice constante at a given concentration. $b_{SR}$ indicates the change in band gap due to the alloy relaxation. In this contribution, the atomic

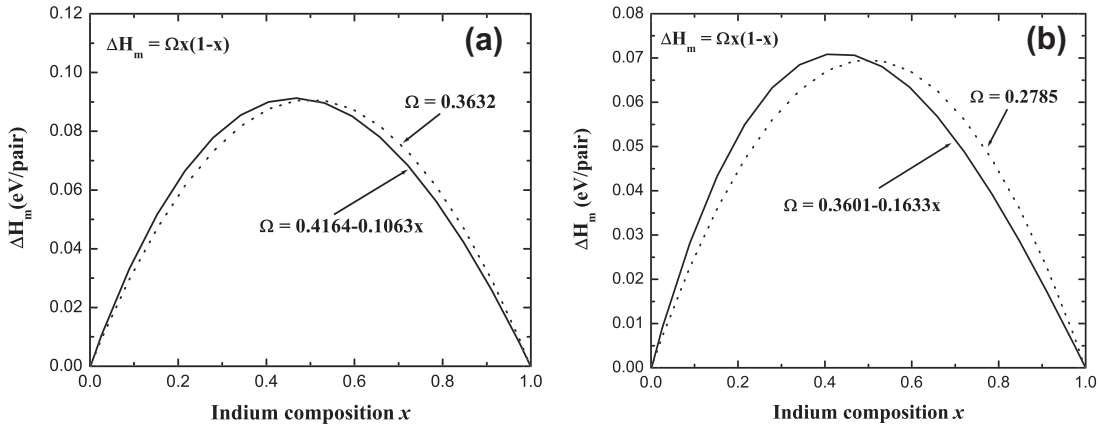


**Fig. 5.** (a) LDA and (b) PBE mixing enthalpy $\Delta H_m$ per cation–anion pair as a function of indium concentration for zinc-blende $Sc_{1-x}In_xP$ alloys. Solid and dotted curves indicate $\Delta H_m$ with the $x$-dependent and $x$-independent interaction parameters $\Omega$, respectively.

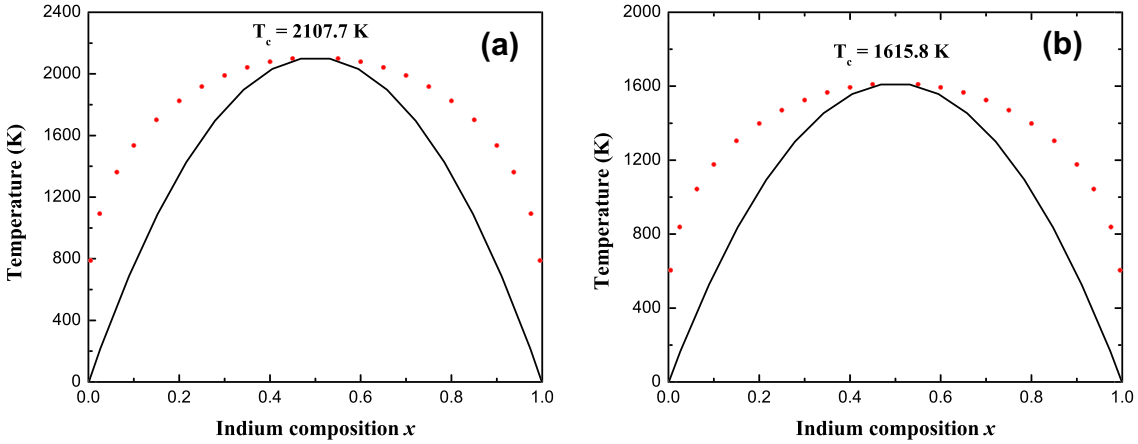


**Fig. 6.** (a) LDA and (b) PBE phase diagrams as a function of indium concentration for zinc-blende $Sc_{1-x}In_xP$ alloys. Solid line indicate $T-x$-dependent spinodal curve and red doted line is the $T-x$-dependent binodal curve. (For interpretation of the references to color in this figure legend, the reader is referred to the web version of this article.)

relaxation originate band mixing. The contribution $b_{SR}$ to the band-gap bowing can be determined by the equation

$$b_{SR} = \frac{E_g^{Sc_{1-x}In_xP}(a) - E_g^{Sc_{1-x}In_xP}(a_{eq})}{x(1-x)}. \quad (8)$$

The total band-gap bowing parameter $b$ is obtained by adding the contributions previously described, so that

$$b = b_{VD} + b_{CE} + b_{SR}. \quad (9)$$

All energies were calculated separately performing band structure calculations using the three LDA, PBE and EV functionals. Fig. 3 shows the calculated band-gap bowing parameters $b$ together with the three different contributions for the $\Gamma \rightarrow \Gamma$ band-gaps as a function of the indium composition for $Sc_{1-x}In_xP$ alloys. Similar results are plotted in Fig. 4 for the $X \rightarrow X$ band gaps. Our results show a similar behavior of the contributions to the total gap bowing obtained with the three LDA, PBE and EV functionals. We observe that the charge exchange effect ($b_{CE}$) is the main contribution to the total gap bowing of $Sc_{1-x}In_xP$ alloys. This is due to a large value of the electronegativity difference (0.42) between those of In (1.78) and Sc atoms (1.36) [42]. A very small volumen deformation ($b_{VD}$) was presented for $Sc_{1-x}In_xP$ alloys due to that the lattice constants of the two binary constituents are very close in the zinc-blende phase. A negligible contribution of the structural relaxation ($b_{SR}$) was obtained, and it is attributed to the similar values of the cationic covalent radii of In (1.44 Å) and Sc (1.44 Å) atoms [42].

We observe that the calculated band-gap bowings with EV functional are larger than the obtained values with both PBE and LDA potentials. An increase of the $\Gamma \rightarrow \Gamma$ band-gap bowings with the increase of the composition is observed in Fig. 3, while $X \rightarrow X$ band-gap bowings show a decrease with In-composition (see Fig. 4).

### 3.3. Enthalpy of mixing and phase diagram

In order to study the phase stability of $Sc_{1-x}In_xP$ alloy, we calculated the phase diagram based on the regular-solution model [43]. The Gibbs free energy of mixing for the zinc-blende $Sc_{1-x}In_xP$ alloy is expressed by the following expression:

$$\Delta G_m = \Delta H_m - T\Delta S_m, \quad (10)$$

where $\Delta H_m$ and $\Delta S_m$ are the enthalpy and entropy of mixing, respectively. $T$ is the absolute temperature. The mixing enthalpy of $Sc_{1-x}In_xP$ alloy can be obtained from the calculated total energies by the expression

$$\Delta H_m = E_{tot}^{Sc_{1-x}In_xP} - xE_{tot}^{InP} - (1-x)E_{tot}^{ScP}. \quad (11)$$

The mixing enthalpy $\Delta H_m$ can also be expressed as

$$\Delta H_m = \Omega x(1-x), \tag{12}$$

where $\Omega$ is the interaction parameter which depends on the material. Using Eqs. (11) and (12), we have calculated $\Omega$ values (per cation–anion pair) at different compositions. The $x$-dependent interaction parameter is obtained from a linear fit to the $\Omega$ values. The linear fit gives $\Omega = 0.4164 - 0.1063x$ eV/pair and $\Omega = 0.3601 - 0.1633x$ eV/pair for LDA and PBE, respectively. The average values of the $x$-dependent $\Omega$ in the range $0 \leqslant x \leqslant 1$ calculated from these equations are 0.3632 eV/pair and 0.2785 eV/pair, respectively. We observe a larger interaction parameter for LDA compared with that of PBE, this can be associated with larger equilibrium energies and with the smaller difference between the equilibrium energies of the constituent binary, obtained with LDA. Using linear $x$-dependent and average values of the interaction parameter, we draw the mixing enthalpies of $Sc_{1-x}In_xP$ alloys for both LDA and PBE functionals. The linear $x$-dependent interaction parameters are used to draw $\Delta H_m$, as shown by the solid curve in Fig. 5a and b. Additionally, we draw $\Delta H_m$ using the average values of the $x$-independent $\Omega$, as shown by the dotted curve in Fig. 5a and b. This last curve is symmetric around $x = 0.5$, while the curve with the $x$-dependent $\Omega$ is asymmetric showing a deviation toward smaller values of $x$-composition. The formation energies are all positive indicating that the system has tendency to segregate in their constituents at low temperature. Higher enthalpies are obtained with LDA than with PBE, and a smaller deviation of $\Delta H_m$ ($x$-dependent $\Omega$) from $\Delta H_m$ ($x$-independent $\Omega$) is observed for LDA. Our mixing enthalpy shows a qualitative behavior similar to other ternary alloys [44].

The mixing entropy $\Delta S_m$ is defined as

$$\Delta S_m = -R[x\ln x + (1-x)\ln(1-x)], \tag{13}$$

where $R$ is the perfect gas constant. Using Eqs. (10)–(13), we calculate $T-x$-dependent $\Delta G_m$, it used to construct the $T-x$ phase diagram which predicts stable, metastable, and unstable mixing zones of $Sc_{1-x}In_xP$ alloy. The critical temperature occurs at a point where both the first and second derivatives of the free energy are zero, i.e., there is no curvature. At a temperature lower than the critical alloy formation temperature $T_c$, the two binodal points are determined as those points at which the common tangent line touches the $\Delta G_m$ curves. The two spinodal points are determined as those points at which the second derivative of $\Delta G_m$ is zero. The resulting phase diagrams of $Sc_{1-x}In_xP$ alloys for LDA and PBE are plotted in Fig. 6a and b. We have calculated the phase diagram using the average values of $x$-dependent $\Omega$, hence the phase diagram looks symmetric. We observe a critical alloy formation temperature of $Tc = 2107.7$ K and $Tc = 1615.8$ K with LDA and PBE, respectively, for zinc-blende $Sc_{1-x}In_xP$ alloys. The spinodal curve in the phase diagram indicates the $T$-dependent equilibrium solubility limit, i.e., the miscibility gap. For temperatures and compositions above this curve a homogeneous alloy is predicted. The wide range between spinodal and bimodal curves indicates that this alloy may exist as a metastable phase. Our phase diagram indicates that the $Sc_{1-x}In_xP$ alloy is stable at high temperature for both LDA and PBE potentials. The large enthalpy value of $Sc_{1-x}In_xP$ alloy suggests a large value of $\Omega$, and consequently a high critical temperature. The calculated $\Delta H_m$, $\Omega$, and $T_C$ values using LDA are larger than those obtained with PBE, due to the smaller difference between the equilibrium energies of the constituent binary, calculated with LDA. Our phase diagram shows a qualitative behavior similar to other ternary alloys [45,46].

## 4. Conclusions

The structural, electronic and thermodynamic properties of zinc-blende $Sc_{1-x}In_xP$ alloys have been studied using the LDA and GGA approaches of DFT within a LAPW scheme. It is found that LDA results of lattice constant and bulk modulus of binary compounds are closer to the experimental values. The lattice parameters of the $Sc_{1-x}In_xP$ alloy increase with indium concentration, showing a negative deviation from Vegard's law. The bulk modulus decreases with composition $x$, showing a small deviation from LCD approach.

We have confirmed that LDA, PBE and EV functionals underestimate the gap energy in semiconductors and that the EV functional reproduces larger values. The InP is a direct semiconductor ($\Gamma \to \Gamma$), while ScP is a direct semiconductor ($X \to X$) in zinc-blenda phase. Our results predict that the band-gap shows a $x$-dependent non-linear behavior. Calculated band gaps shows a transition from $X \to X$ to $\Gamma \to \Gamma$ at a especial concentration $x$. We have found that the main contribution to the total bowing parameter comes from the large difference in electronegativity between indium and scandium atoms. These results show the importance of combining ScP with InP for the band gap engineering.

On the other hand, the calculated phase diagrams indicate a significant phase miscibility gap with a critical temperature of 2107.7 K and 1615.8 K for LDA and PBE, respectively. In both cases these results indicate that the $Sc_{1-x}In_xP$ alloy is unstable over a wide range of intermediate compositions at normal growth temperatures and that is stable at hight temperature.

These results predict that zinc-blende $Sc_{1-x}In_xP$ alloys are good candidates to be employed in the design and production of optoelectronic devices in the near future. In the absence of experimental works for these alloys, our results can be useful for further studies.

## Acknowledgements

This work was supported by DIDI-Universidad del Norte. The calculations reported in this paper were performed using the computing facilities of the HIPERLAB-cluster at the Universidad del Norte.

## References

[1] Sadao Adachi, Properties of Semiconductor Alloys: Group-IV, IIIV and IIVI Semiconductors, Wiley Series in Materials for Electronic and Optoelectronic Applications, John Wiley and Sons Ltd., 2009.
[2] V. Swaminathan, in: A. Katz (Ed.), Indium Phosphide and Related Materials: Processing, Technology, and Devices, Artech House, Boston, 1992.
[3] V. Swaminathan, A.T. Macrander, Materials Aspects of GaAs and InP Based Structures, Prentice Hall, Englewood Cliffs, NJ, 1991.
[4] T.J. Coutts, S. Naseem, Appl. Phys. Lett. 46 (1985) 364.
[5] M.B. Spitzer, C.J. Keavney, S.M. Vernon, V.E. Haven, Appl. Phys. Lett. 51 (1987) 364.
[6] V. Korobov, M. Leibovitch, Yoram Shapira, Appl. Phys. Lett. 74 (1993) 3251.
[7] J. Wang, M.K. Gudiksen, X. Duan, Y. Cui, C.M. Lieber, Science 293 (2001) 1455.
[8] Koichi Murata, Kimikazu Sano, Hiroyuki Fukuyama, Toshihiko Kosugi, Makoto Nakamura, Hirohiko Sugahara, Masami Tokumitsu, Takatomo Enoki, Thin Solid Films 515 (2007) 4313.
[9] M.V.V.M. Satya Kishore, U.V. Varadaraju, J. Power Sources 156 (2006) 594.
[10] Carmen S. Menoni, Ian L. Spain, Phys. Rev. B 35 (1987) 7520.
[11] D. Nichols, D. Rimai, R. Sladek, Solid State Commun. 36 (1980) 667.
[12] R. Trommer, H. Muller, M. Cardona, P. Vogl, Phys. Rev. B 21 (1980) 4869.
[13] P. Rochon, E. Fortin, Phys. Rev. B 12 (1975) 5803.
[14] W.M. Yim, E.J. Stofko, R.T. Smith, J. Appl. Phys. 43 (1972) 254.
[15] Rashid Ahmed, Fazal-e-Aleem, S. Javad Hashemifar, Hadi Akbarzadeh, Physica B 403 (2008) 1876.
[16] A. Bouhemadou, R. Khenata, M. Kharoubi, T. Seddik, Ali H. Reshak, Y. Al-Douri, Comput. Mater. Sci. 45 (2009) 474.
[17] A. Mujica, R.J. Needs, Phys. Rev. B. 55 (1997) 9659.
[18] P.E. Van Camp, V.E. Van Doren, J.T. Devreese, Phys. Rev. B 41 (1990) 1598.
[19] N. Bouarissa, Solid-State Electron. 44 (2000) 2193.
[20] O. Arbouche, B. Belgoumene, B. Soudini, Y. Azzaz, H. Bendaoud, K. Amara, Comput. Mater. Sci. 47 (2010) 685.
[21] A. Maachou, B. Amrani, M. Driz, Physica B 388 (2007) 384.
[22] Wenhui Xue, You Yu, Yuna Zhao, HuiLei Han, Tao Gao, Comput. Mater. Sci. 45 (2009) 1025.
[23] S. Ugur, F. Soyalp, Solid State Commun. 147 (2008) 198.
[24] K. Iga, S. Kinoshita, Process Technology for Semiconductor Lasers, Springer-Verlag, Berlin, 1996.

[25] M. Quillec, Materials for Optoelectronics, Kluwer Academic Publ, Boston, 1996.
[26] U.K. Mishra, J. Singh, Semiconductor Device Physics and Design, Springer, Dordrecht, 2008.
[27] M. Othman, E. Kasap, N. Korozlu, Physica B 405 (2010) 2357.
[28] Mohammed Ameri, Ali Bentouaf, Mohammed Doui-Aici, Rabah Khenata, Fatima Boufadi, Amina Touia, Mater. Sci. Appl. 2 (2011) 729.
[29] Alex Zunger, S.H. Wei, L.G. Ferreira, James E. Bernard, Phys. Rev. Lett. 65 (1990) 353.
[30] P. Blaha, K. Schwarz, G.K.H. Madsen, D. Kvasnicka, J. Luitz, WIEN2k, an Augmented Plane Wave plus Local Orbital Program for Calculating Crystal Properties, Vienna University of Technology, Vienna, Austria, 2001.
[31] P. Hohenberg, W. Kohn, Phys. Rev. 136 (1964) 864.
[32] W. Kohn, L.J. Sham, Phys. Rev. 140 (1965) 1163.
[33] J.P. Perdew, Y. Wang, Phys. Rev. B 45 (1992) 13244.
[34] J.P. Perdew, K. Burke, M. Emzerhof, Phys. Rev. Lett. 77 (1996) 3865.
[35] E. Engel, S.H. Vosko, Phys. Rev. B 47 (1993) 13164.
[36] F.D. Murnaghan, Proc. Natl. Acad. Sci. USA 30 (9) (1944) 244.
[37] L. Vegard, Z. Phys. 5 (1921) 17.
[38] B. Jobst, D. Hommel, U. Lunz, T. Gerhard, G. Landwehr, Appl. Phys. Lett. 69 (1996) 97.
[39] A.R. Denton, N.W. Ashcroft, Phys. Rev. A 43 (1991) 3161.
[40] Philipp Dufek, Peter Blaha, Karlheinz Schwarz, Phys. Rev. B 50 (1994) 7279.
[41] J.E. Bernard, A. Zunger, Phys. Rev. B 36 (1987) 3199.
[42] W. Sargent, Table of Periodic Properties of the Elements, Sargent-Welch Scientific, Skokie, IL, 1980.
[43] R.A. Swalin, Thermodynamics of Solids, Wiley, New York, 1961.
[44] F. El Haj Hassan, A. Breidi, S. Ghemid, B. Amrani, H. Meradji, O. Pages, J. Alloys Compd. 499 (2010) 80.
[45] F. El Haj Hassan, H. Akbarzadeh, Mater. Sci. Eng. B 121 (2005) 170.
[46] M. Ferhat, F. Bechstedt, Phys. Rev. B 65 (2002) 75213.